ChemPubSoc Europe

DOI: 10.1002/ejic.201600468

EurJIC European Journal of Inorganic Chemistry

Full Paper

DNA Photoprobes

Design and Photophysical Studies of Acridine-Based Ru^{II} Complexes for Applications as DNA Photoprobes

Quentin Deraedt,[a] Lionel Marcélis,[a] Thomas Auvray,[b] Garry S. Hanan,[b] Frédérique Loiseau,[c] and Benjamin Elias*[a]

Abstract: A series of new extended planar aromatic ligands based on an acridine core (dpac = dipyrido[3,2-*a*:2′,3′-*c*]-acridine; $dpacF_2$ = 7,8-difluorodipyrido[3,2-*a*:2′,3′-*c*]acridine; $dpacF_4$ = 6,7,8,9-tetrafluorodipyrido[3,2-*a*:2′,3′-*c*]acridine) and their respective Ru^{II} complexes were synthesized and extensively studied. The photophysical and theoretical studies revealed that Ru-DPAC and Ru-$DPACF_2$ allow emission from a $^3MLCT_{phen/dpac}$ excited state at 597 and 604 nm, respectively, whereas the lowest excited state for Ru-$DPACF_4$ shifts from a bright $^3MLCT_{phen/dpac}$ state towards a poorly luminescent $^3MLCT_{dpac}$ state (λ_{em} = 609 nm) owing to the formation of hydrogen bonds with water molecules in the excited state. These complexes exhibit up to sevenfold luminescence enhancement in the presence of complementary and mismatched DNA, demonstrating a strong binding to polynucleotides. The results emphasize the interest in Ru^{II} complexes bearing acridine derivatives as DNA interacting agents as a complement to the well-known phenazine-based derivatives.

Introduction

Transition-metal complexes are of great interest in molecular biology and biochemistry.[1] In addition to being present as coordination sites in proteins or cofactors in Nature, these compounds offer numerous advantages for their use as photoprobes or photoreagents, such as DNA interacting agents. Indeed, the great modularity of the properties of the transition-metal complexes makes them ideal in this scope. Polypyridyl Ru^{II} complexes have been the subject of considerable interest for the past few decades. Even though numerous publications describe their use as catalysts,[2] or as energy conversion and storage devices,[3] these Ru^{II} complexes also appear to be relevant in the context of biological applications such as sensing[4] and therapeutic agents.[5] Among them, Ru^{II} complexes bearing the intercalating dppz ligand (dppz = dipyrido[3,2-*a*:2′,3′-*c*]phenazine) have been studied for the last twenty-five years. Indeed, $[Ru(bpy)_2dppz]^{2+}$ and $[Ru(phen)_2dppz]^{2+}$ (bpy = bipyridine, phen = phenanthroline) bind readily to DNA ($K_{aff} \approx 10^6$ L mol^{-1}) and display intense luminescence in the presence of DNA, whereas the luminescence of the complex alone is switched off in aqueous media.[6] This "light switch" behavior has been ascribed to the population of a mixture of excited metal-to-ligand charge-transfer states (MLCT states) where the electron located on the dppz ligand is either proximal or distal from the metallic center.[7] In water, a quenching occurs through the formation of hydrogen bonds with the phenazine core of the dppz, whereas upon intercalation into DNA, the luminescence of the complex is restored, as observed in organic media.[8] In addition, studies with mismatch containing DNA show correlation between the luminescence increase of $[Ru(bpy)_2dppz]^{2+}$ and the mismatch thermodynamic stability.[9] These environment-sensitive optical properties render dppz-based Ru^{II} complexes potent candidates as photoprobes for different DNA topologies.

Although complexes based on dppz derivatives and other ligands incorporating a phenazine core have received a lot of attention, fewer studies have been reported on complexes based on ligands incorporating an acridine core. Studies on the tpac ligand (tpac = tetrapyrido[3,2-*a*:2′,3′-*c*:3″,2″-*h*:2‴,3‴-*j*]acridine)[10] and the corresponding complexes[11] showed that the acridine core induces notable modifications to the behavior of the resulting complex compared with the phenazine-based equivalent. Analogous to dppz, the dpac ligand (dpac = dipyrido[3,2-*a*:2′,3′-*c*]acridine) and its Ru^{II} complex have been only recently reported and the latter was shown to be a potent nicotinamide (NAD) derivative for electron storage systems.[12] However, its photophysical properties were not fully investigated and its interaction with DNA was not studied. Furthermore, as dpac bears one less non-chelating nitrogen atom than dppz, only one hydrogen bond with solvent molecules in the excited state would be possible, suggesting potential differences with dppz-based Ru^{II} complexes.

In this context, our work focuses on the synthesis of a series of extended planar aromatic ligands based on the acridine core {dpac (**4**); $dpacF_2$ = 7,8-difluorodipyrido[3,2-*a*:2′,3′-*c*]acridine (**5**);

[a] *Institute of Condensed Matter and Nanosciences, Molecules, Solids and Reactivity (IMCN/MOST), Université Catholique de Louvain, Place Louis Pasteur 1/L4.01.02, 1348 Louvain-la-Neuve, Belgium*
E-mail: Benjamin.Elias@uclouvain.be
http://www.uclouvain.be/en-237299.html
[b] *Département de Chimie, Université de Montréal, 2900 Edouard-Montpetit, Montréal, Québec H3T-1J4, Canada*
[c] *Département de Chimie Moléculaire, Université Grenoble-Alpes, CNRS UMR 5250, BP53 38041 Grenoble, France*

Supporting information and ORCID(s) from the author(s) for this article are available on the WWW under http://dx.doi.org/10.1002/ejic.201600468.

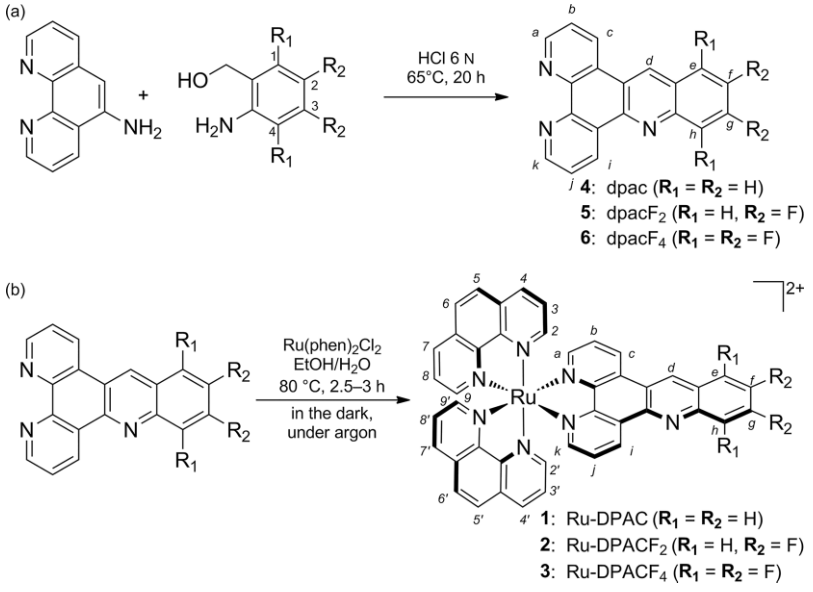

Figure 1. Synthetic scheme of dpac ligands and their corresponding Ru^{II} complexes.

$dpacF_4$ = 6,7,8,9-tetrafluorodipyrido[3,2-*a*:2′,3′-*c*]acridine (**6**)}, and the study of their respective Ru^{II} complexes {Ru-DPAC for $[Ru(phen)_2dpac]^{2+}$ (**1**); Ru-DPACF$_2$ for $[Ru(phen)_2dpacF_2]^{2+}$ (**2**); Ru-DPACF$_4$ for $[Ru(phen)_2dpacF_4]^{2+}$ (**3**)} (Figure 1). In this paper, we report an extensive theoretical and experimental study on these complexes and analyze the influence of the acridine core on the photophysical properties and DNA interactions of the resulting Ru^{II} complexes compared with dppz-based complexes. We also investigate the selectivity for Ru-DPAC to probe DNA mismatches.

Results and Discussion

Synthesis

The acridine core can be obtained through numerous synthetic pathways, such as Skraup cyclization,[24] self-condensation,[10] Cu^0, Pd^0, or Zn^{II}-based organometallic couplings,[25] and cycloadditions.[26] In our case, a Tröger's base modified synthetic scheme was found to be successful and allowed us to obtain dpac and its fluoro derivatives with high yields (Figure 1). The synthetic methodology consisted of a cyclization between 5-amino-1,10-phenanthroline and the appropriate *o*-aminobenzyl alcohols.[10,27]

The corresponding Ru^{II} complexes were synthesized by the direct chelation of the extended ligand onto a Ru^{II} precursor (Figure 1) by using methodologies previously described for similar compounds. All the intermediate and final compounds were protected from direct light during the synthesis and purification steps to prevent photochemical degradation. The reactions were performed under argon to avoid any oxidation of the metal center.

The complexes were fully characterized by HRMS and ^1H NMR spectroscopy (see the Experimental Section and the Supporting Information). Not all the multiplicity and coupling constants can be determined owing to the superposition of several signals and/or lack of fine resolution for some peaks in the ^1H NMR spectra. The ^1H NMR spectra show unambiguously the absence of symmetry elements for all the complexes, which induces the non-equivalence of (i) the protons on the extended planar ligand and (ii) the ancillary ligands. The ^1H NMR spectra are sensitive to concentration as some shifts occurred upon changes in the concentration. For solubility purposes, all the complexes were converted into the chloride salt for experiments conducted in water or buffer or to the hexafluorophosphate salt for studies in organic solvents.

Electrochemistry

The electrochemical data for the three complexes were obtained by cyclic voltammetry in dry deoxygenated MeCN or *N*,*N*-dimethylformamide (Table 1). Complexes **1**–**3** display a one-electron reversible oxidation wave at a potential close to that of the Ru^{2+}/Ru^{3+} oxidation of $[Ru(phen)_3]^{2+}$.[28] This similarity between the oxidation potentials of all these complexes confirms the metal-based nature of the process ($Ru^{2+/}Ru^{3+}$ redox couple) irrespective of the substitution on the extended planar ligand. Three reduction waves are monitored for each complex. From the comparison with the reduction potentials of $[Ru(phen)_3]^{2+}$ (–1.30 V vs. Ag/AgCl)[29] and $[Ru(phen)_2dppz]^{2+}$ (Ru-DPPZ; –0.95 V vs. Ag/AgCl),[29] the first reduction of the five complexes is attributed to the addition of one electron to the extended planar ligand. The anodic shift observed for Ru-DPACF$_4$ (–0.97 V vs. Ag/AgCl) indicates greater stabilization of the π* orbital centered on the dpacF$_4$ ligand with respect to that of Ru-DPAC and Ru-DPACF$_2$. The next two reduction waves are attributed to successive reduction of the two ancillary phen ligands. The potentials in the excited state (namely, E_{ox}* and E_{red}*) for the three complexes have been estimated from the ground-state redox potentials and the energy of the excited state corresponds to the maximum of the emission spectrum at 298 K (see below). Not surprisingly, Ru-DPACF$_4$ (E_{red}* =

+1.07 V vs. Ag/AgCl) is the most oxidizing complex in the excited state.

Table 1. Potentials for the oxidation ($E_{1/2\ ox}$) and reduction ($E_{1/2\ red}$) of complexes **1**–**3**.

	$E_{1/2\ ox}$[a] [V vs. Ag/AgCl]	$E_{1/2\ red}$[a,b] [V vs. Ag/AgCl]	$\lambda_{max\ em}$[a] [nm]	E_{ox}*[c] [V vs. Ag/AgCl]	E_{red}*[d] [V vs. Ag/AgCl]
$[Ru(phen)_3]^{2+}$	1.32	−1.30	604	−0.73	0.70
		−1.47			
		−1.68			
Ru-DPPZ[30]	1.35	−0.95	618	−0.67	1.02
		−1.39			
Ru-DPAC	1.35	−1.22	597	−0.73	0.86
		−1.35			
		−1.66			
Ru-DPACF$_2$	1.35	−1.15	604	−0.71	0.91
		−1.34			
		−1.62			
Ru-DPACF$_4$	1.35	−0.97	609	−0.69	1.07
		−1.30			
		−1.52			

[a] Measured in dry acetonitrile. [b] The reversibility of the reduction processes being not able to be determined due to adsorption of the reduced species on the electrode suface, $E_{1/2}$ has been estimated from the reduction peak. [c] The excited-state oxidation potential was estimated from the ground-state oxidation potential and the energy of the emission maximum with the equation $E_{ox}^* = E_{1/2\ ox} - E_{0-0} \approx E_{1/2\ ox} - \Delta E_{\lambda max,\ em}$. [d] The excited-state reduction potential was estimated from the ground-state reduction potential and the energy of the emission maximum with the equation $E_{red}^* = E_{1/2\ red} + E_{0-0} \approx E_{1/2\ red} + \Delta E_{\lambda max,\ em}$.

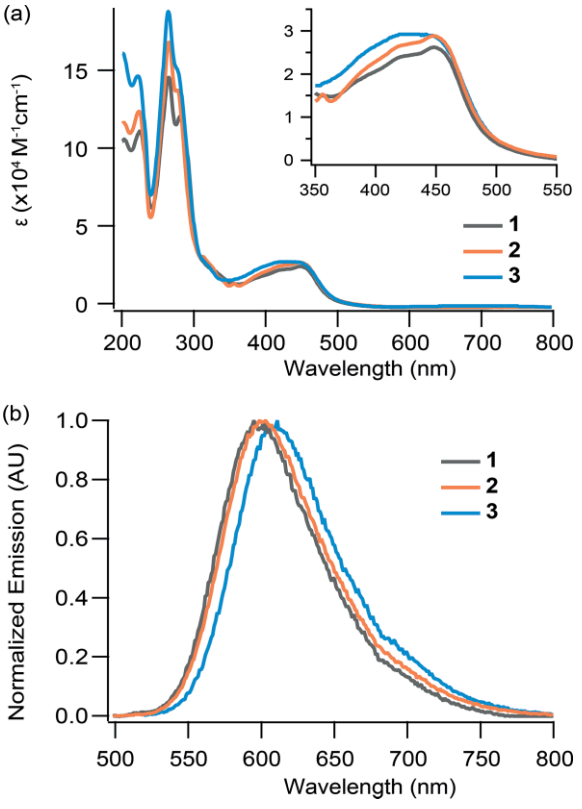

Figure 2. (a) Absorption and (b) emission spectra (λ_{exc} = 448 nm) of **1** (gray), **2** (orange), and **3** (blue) in acetonitrile under air at room temperature. Inset of a: Absorption bands corresponding to MLCT transitions.

Absorption Spectra and Computational Studies

The absorption data at ambient temperature in water and acetonitrile, under air and under argon for the three complexes, as well as for other complexes for comparison purposes, are listed in Table 2. Absorption spectra for all complexes in acetonitrile are depicted in Figure 2, a. The absorption of Ru^{II} complexes generally corresponds to the superposition of different transitions involving either the ligands or both the metal and the ligand.[31] In the present case, comparison with literature and absorption spectra of the free ligands allowed us to assign the intense absorption ($\varepsilon \geq 10^5$ M^{-1} cm^{-1}) bands in the UV region to ligand-centered (LC) transitions and the ones in the visible region ($\varepsilon \approx 10^4$ M^{-1} cm^{-1} around $\lambda \approx 400$ nm) to metal-to-ligand charge-transfer (MLCT) transitions, where L = phen ($^1MLCT_{phen}$) and dpac ($^1MLCT_{dpac}$).

In the case of Ru-DPPZ, the absorption of a photon leads to the formation of a charge-separated state, Ru^{3+}/dppz$^{\bullet-}$, in which an electron is transferred from the metal center towards either the phen or phenazine part of the dppz ligand depending on the environment of the complex.[32] This accounts for the peculiar photophysical behavior of Ru-DPPZ. In our case, exchanging the phenazine core with an acridine, that is, replacing a nitrogen atom with a carbon atom, should influence the electronic transitions involved in the formation of the excited state. Strikingly, a sole small bathochromic shift ($\Delta\lambda$ = 8 nm) of the MLCT band is observed for **1**–**3** compared with Ru-DPPZ.

To get more information on the photophysical scheme of our complexes, **1**–**3** as well as Ru-DPPZ were studied computationally. The ground- and vertical excited-state electronic structures were investigated by means of DFT/time-dependent (TD)-DFT calculations by using the hybrid PBE0 functional and the

Table 2. Absorption data for complexes **1**–**3** in CH_3CN and H_2O at 298 K in aerated or deaerated solution.

	Absorbance λ_{max} [nm] (ε [10^4 M^{-1} cm^{-1}])[a] MeCN	H_2O
$[Ru(phen)_3]^{2+}$	418, 447 (1.84)	419, 447 (1.83)
Ru-DPPZ[30]	221, 264, 370, 440 (2.34)	220, 264, 368, 440
Ru-DPAC (**1**)	224 (15.1), 264 (16.3), 280 (11.6), 448 (2.62)	224 (15.1), 264 (16.2), 280 (11.6), 448 (2.62)
Ru-DPACF$_2$ (**2**)	223 (16.2), 264 (19.0), 278 (14.4), 448 (2.88)	223 (16.1), 264 (19.0), 278 (14.3), 448 (2.88)
Ru-DPACF$_4$ (**3**)	221 (17.1), 264 (18.9), 279 (14.0), 448 (2.87)	221 (17.0), 264 (18.9), 279 (14.1), 448 (2.88)

[a] Measurements made with solutions with 1×10^{-5} mol L^{-1} of the complex at room temperature.

LanL2DZ basis set. The solvent (MeCN or H_2O) is included by a conductor-like polarizable continuum model.[33] With this system, the first runs of calculations performed with water did not account for the experimental differences when going from acetonitrile to water. A similar observation was made by Daniel et al. who overcame the limitation of the continuum model, which does not describe specific interactions, such as nitrogen–hydrogen bond interactions, by using a discrete model.[23] Water molecules are thus added without any constraint on their position before geometry optimization and calculations.

The energy diagram for the different compounds is presented in Figure 3 (further details on the electronic structures can be found in Tables S2–S7 in the Supporting Information). For the sake of clarity, throughout the manuscript the electron-accepting portion of the extended ligands is underlined to differentiate the two moieties that are suggested to participate in the relaxation processes. The contributions of each moiety of the complexes are depicted in different colors; in particular, the phenanthroline part of the extended ligand (dpac, green) and the terminal fragment (dpac/dppz, orange) are differentiated in order to discuss their respective contributions. Regardless of the solvent, the introduction of electron-withdrawing fluoride modifies the electronic repartition in the ground state. Although it has only a little effect on the Ru (red) and ancillary phen (blue) centered orbitals, it strongly stabilizes the levels centered on the dpac/dppz ligands. In addition, as the number of fluoride atoms increases, the dpac contribution increases in the LUMO whereas the dpac contribution increases in the LUMO + 1.

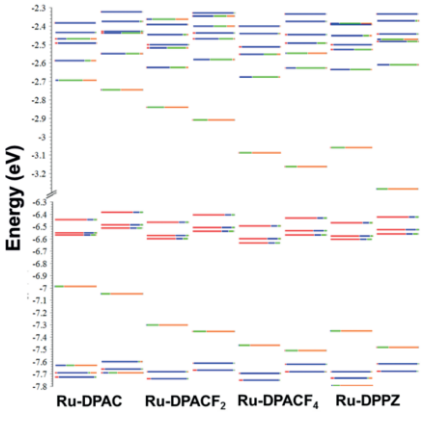

Figure 3. Energy diagram of the complexes **1**–**3** and Ru-DPPZ. Fragment contributions are reported with different colors: Ru in red, ancillary phen in blue, dpac/dppz in green, dpac/dppz in orange. Solvent used: left = MeCN, right = H_2O.

The experimental absorption spectra matched well with the calculated transitions, allowing us to attribute the different transitions by using natural transitions orbitals (NTOs)[34] (see Figures S19–S21). When comparing the absorption spectra of the different complexes in acetonitrile, one can observe that there are no major differences in the position and intensities of the absorption maxima. Indeed, in all cases the $^1MLCT_{phen}$ are the main transitions in the visible part of the spectra (400–550 nm); transitions involving the $^1MLCT_{dpac}$ and $^1MLCT_{dpac/dppz}$ of lower intensities are redshifted as the number of fluoride atoms increases, but this does not affect the final absorption spectra. A similar explanation can be used to account for the similarity between the absorption spectra in acetonitrile and water. As the polarity of the solvent increases, the levels centered on the metal and ancillary phen are equally destabilized, leaving the $^1MLCT_{phen}$ unchanged whereas the dpac/dppz orbitals are stabilized, leading to a redshift of the $^1MLCT_{dpac/dppz}$ and $^1MLCT_{dpac/dppz}$ transitions. These shifts are, however, small, as seen in Table 2.

Emission Spectra, Lifetimes, Quantum Yields, and Computational Studies

All our complexes display broad unstructured emission (Figure 2, b), typical of a ^3MLCT-type excited state, both in organic solvent and water. The luminescence lifetimes and the quantum yields of luminescence for each complex were measured in water and acetonitrile under an inert atmosphere (Table 3). The large k_r values ($> 10^4$ s^{-1}, Table 3), the positive solvatochromic effect ($\Delta\lambda \approx +20$ nm when going from CH_2Cl_2 to water, data not shown) and the hypsochromic shift of the emission band at 77 K (see Figure S3) confirm the charge-transfer character of the excited state. It is worth mentioning that, in air-equilibrated solvents, a decrease in the luminescence intensity with respect to degassed solutions is systematically observed, indicating a quenching by oxygen (see Table S1). We expect that, as for other Ru^{II} complexes, an efficient photosensitization of $^3O_2$ by the excited Ru^{II} complexes is occurring.[35] Other quenching mechanisms such as electron transfer to form superoxide anions may also occur, but are beyond the scope of this study.

The emission maxima are almost identical for Ru-DPAC and Ru-DPACF$_2$; the addition of the two fluorine atoms onto the

Table 3. Emission data for complexes **1**–**3**.

	Emission $\lambda_{em\ max}$ [nm][a,b]		Emission λ_{max} at 77 K [nm]	Φ_{em}[a,c,d]		τ_{em} [ns][d]		k_r [10^3 s^{-1}][d]		k_r [10^5 s^{-1}][d]	
	MeCN	H_2O	EtOH/MeOH, 4:1	MeCN	H_2O	MeCN	H_2O	MeCN	H_2O	MeCN	H_2O
$[Ru(phen)_3]^{2+}$	604	606	564[36]	0.028	0.072	460	920	60.9	75.0	21	9.7
Ru-DPPZ[30]	618	–*	580[7d]	0.033	–*	663	–*	49.8	–*	15	–*
Ru-DPAC	597	604	567	0.038	0.066	710	999	53.5	66.1	14	9.4
Ru-DPACF$_2$	604	607	573	0.052	0.189	875	958	59.4	197.3	11	8.5
Ru-DPACF$_4$	609	611	568	0.084	0.050	915	238	91.8	210.1	10	40

[a] Measurements made with solutions with 1×10^{-5} mol L^{-1} of the complex. [b] Measurements made under ambient air conditions. [c] The quantum yield of luminescence is calculated relative to that of $[Ru(bpy)_3]^{2+}$ in an aerated aqueous solution ($\Phi_{em}^{air} = 0.028$).[28] [d] Quantum yield of luminescence, luminescence lifetimes and radiative rate constants are determined under an argon atmosphere. Errors estimated to 10 %. * No luminescence was observed in H_2O.

dpac ligand has thus only a small influence on the energy difference between the ^{3}MLCT and the ground state, whereas this energy decreases for Ru-DPACF$_4$. This observation is in agreement with the decrease in energy of the π* orbital centered on the extended planar ligand going to a more electron-withdrawing core. Interestingly, none of these complexes behave like Ru-DPPZ, which is known to have light-switching behavior.

Numerous experimental and theoretical studies have been devoted to understanding the light-switch effect.[4b,7a,36] It is now commonly accepted that this quenching is caused by hydrogen-bonding with water molecules, leading to the stabilization of dark states, such as ^{3}MLCT$_{dppz}$ and ^{3}LC$_{dppz}$, the latter being the lowest triplet state (summarized in Figure 4, c).[37,38] Our calculations led to similar results with a change in the nature of the lowest metal-to-ligand charge-transfer state from a bright ^{3}MLCT$_{phen}$ state in acetonitrile to a more stabilized dark ^{3}MLCT$_{dppz}$ state in water.

In the case of our complexes, Ru-DPAC and Ru-DPACF$_2$ do not present light-switching behavior whereas Ru-DPACF$_4$ partially does as its luminescence is notably reduced in water, as indicated by its smaller quantum yield and larger k_{nr} value in water. Once again, computational studies were used to gain some information to explain this behavior and compare it with Ru-DPPZ. The qualitative results obtained for the triplet TD-DFT calculations were used to draw the photophysical schemes presented in Figure 4 for each situation (for numeric values, see Table S8). The computational studies show that ^{3}LC states centered on dpac/dppz ligands have a lower energy than ^{3}MLCT states for all complexes. The presence of such ^{3}LC states was also reported in computational studies realized previously.[23,35,39] Nevertheless, the experimental characteristics of emission clearly indicate that the luminescence of all Ru^{II} complexes originates from the ^{3}MLCT states and that low-lying ^{3}LC states are not likely to play a role in the deactivation of the ^{1}MLCT states generated upon light irradiation (see Table 3, larger quantum yield of luminescence for complexes **1**–**3** in MeCN compared with [Ru(phen)$_3$]$^{2+}$). Therefore, we focus our discussion on the ^{3}MLCT manifold, which accounts for the photophysical behavior of our complexes.

In acetonitrile, all compounds follow similar trends as in Figure 4 (a). After an ultrafast ISC[40] from ^{1}MLCT states generated upon absorption of photons, ^{3}MLCT states are populated corresponding to charge transfer from the Ru^{II} center towards either the ancillary phen or the phen part of the planar ligand (dpac or dppz). The similar energies of these emissive ^{3}MLCT states explain the similarity of the luminescence maxima observed for all complexes.

In water, complexes **1**–**2** present a stronger emission and are longer lived (see Table 3). Calculations show that the relative energy of each ^{3}MLCT state is not significantly modified and the fragment contributions to each triplet state remain similar to those in MeCN; hence, these compounds behave like [Ru(phen)$_3$]$^{2+}$ and exhibit an increased luminescence in water compared with organic solvent. Complexes **1**–**2** also follow the same photophysical scheme in water as in MeCN (Figure 4, a). In contrast to Ru-DPPZ, where the lowest excited states involve the phenazine core of the dppz, the acridine core in complexes **1**–**2** seems not to be involved and ^{3}MLCT remains localized on the ancillary ligands or the phen moiety of the dpac ligands. We thus propose for these complexes that their lowest excited states are luminescent ^{3}MLCT$_{phen/dpac}$ states. The ^{3}MLCT$_{dpac}$ excited states are assumed to be higher in energy than the ^{3}MLCT$_{phen/dpac}$ ones for these two complexes (in contrast to ^{3}MLCT$_{dppz}$ for Ru-DPPZ), suggesting the acridine core disfavors the charge-separation process in the excited state for **1**–**2**. A similar behavior has been previously observed for TPAC-based mono- and dinuclear Ru^{II} complexes, for which the electrochemical and spectroscopic data indicate that the lowest MLCT transition is a ^{3}MLCT$_{tpac}$ one and that dinucleation affects very slightly these properties. This suggests that the two metallic centers of the dinuclear TPAC-based Ru^{II} complexes behave independently in spite of the conjugated TPAC bridging ligand.[11,41]

In opposition to the former examples, Ru-DPACF$_4$ displays a much shorter luminescence lifetime and lower quantum yield in water than in acetonitrile (Table 3). For this complex, we assume that upon absorption of light, a ^{1}MLCT$_{phen}$ state is formed, which rapidly undergoes an ISC to a luminescent ^{3}MLCT$_{phen/dpac}$ state. Further relaxation occurs on the acridine moiety of the extended planar ligand, leading to the formation of the ^{3}MLCT$_{dpac}$ excited state. In water, there is an interconversion between two excited states: one assigned to the non-hydrogen-bonded excited state dpac, and the other one to a mono-hydrogen-bonded excited state (depicted as dpac-H, in Figure 4, b). The presence of the dpac-H excited state is suggested by the shorter excited state lifetime of this complex in

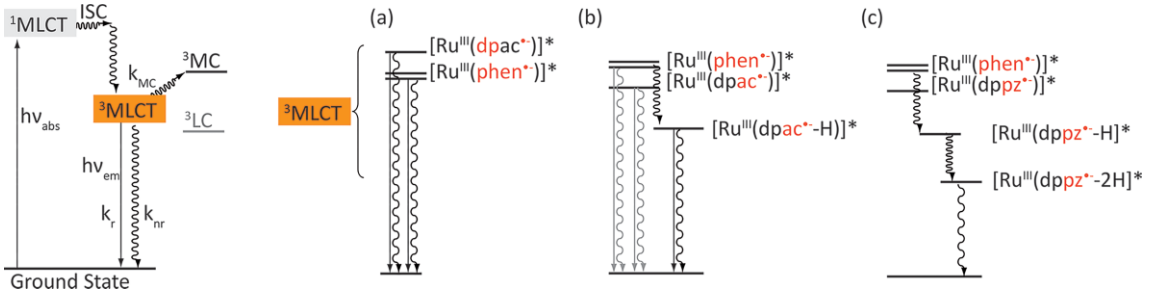

Figure 4. Representation of the photophysical scheme for dpac-based complexes in water. The deactivation of the ^{3}MLCT states is emphasized on the right part of the figure for (a) Ru-DPAC and Ru-DPACF$_2$, (b) Ru-DPACF$_4$, and (c) Ru-DPPZ in water. The photophysical scheme for all complexes (**1**–**3** and Ru-DPPZ) in MeCN can be described as in (a). Solid arrows stand for radiative, wavy arrows stand for non-radiative transitions (intersystem crossing, internal conversion, or vibrational relaxation).

water. In a similar way as described for Ru-DPPZ,[7b] we propose that the excited state localized on dpac, which is higher in energy in aprotic solvents, is stabilized when involved in a hydrogen bond and thus becomes dominant in water. Indeed, protic solvents would stabilize the charge-separated excited state owing to the formation of a hydrogen bond with the free nitrogen atom of the dpacF_4 ligand. The partial quenching of the luminescence of **3** is in agreement with the model proposed by Lincoln and co-workers for which two hydrogen bonds are required for the full luminescence quenching of the excited state of Ru-DPPZ in water. The photophysical behavior of Ru-DPACF_4 thus contrasts with the photophysical properties of Ru-DPAC and Ru-DPACF_2, which are similar to those of $[Ru(phen)_3]^{2+}$.

Photophysical Behavior in the Presence of DNA and Polynucleotides

As mentioned in the Introduction, Ru^{II} complexes are relevant tools to probe DNA. The influence of hydrogen bonds with water on the photophysics of the complex is one of the key parameters in this context, but not the only one at stake. With the notable exception of some photoreactive complexes,[5] polypyridyl Ru^{II} complexes are more luminescent in the presence of DNA. This enhancement of luminescence is due to the association of the complex with DNA, which protects the excited complex from quenching or non-radiative deactivations. If complexes possess one extended planar ligand, a specific interaction is observed with DNA, where the complex is intercalated inside the bases stack. This intercalation mode generally leads to strong association ($K_{aff} \approx 10^6$ L mol^{-1}) and an intense luminescence enhancement of the excited intercalated complex in comparison to the "free" complex left in aqueous media.[7c,8,29,42] Interestingly, Ru-DPPZ is able to distinguish matched and single-base mismatched sites in oligonucleotides. This small sensitivity of the luminescence enhancement in the presence of a mismatch can be correlated to its thermodynamic stability.[9] We thus investigated the ability of our new complexes to probe DNA and some particular topologies, such as different single-base mismatches.

In the presence of increasing concentrations of DNA (CT-DNA and SS-DNA), the luminescence of the dpac complexes **1**–**3** is enhanced (Figure 5). This increase in luminescence for the three complexes is strong and occurs even at a very low ratio of DNA per complex, suggesting a high binding affinity of the complexes for these two DNA types. To determine the binding affinity for these equilibria, we used a modified McGhee–von Hippel equation[43] as an expression for the luminescence intensity as a function of the ratio of Ru^{II} per DNA (I/I_0 vs. [DNA]/[complex], with I_0 the intensity of luminescence in the absence of DNA and [DNA] expressed in base-pair equivalents, see Table 4 and Figure 5). The luminescence enhancement observed presumably results from a decrease in the non-radiative deactivation processes of the ^{3}MLCT excited states. This protection is induced by the double helix microenvironment, which protects the excited complexes from quenching by oxygen. As our extended planar ligands are similar to dppz in terms of structure, we assume our complexes also intercalate into the DNA strands, which is consistent with the binding values obtained.

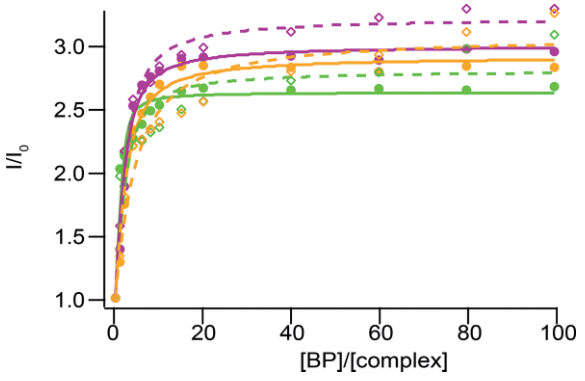

Figure 5. Steady-state luminescence titration (λ_{exc} = 448 nm) of **1** (green), **2** (purple), and **3** (orange) with SS-DNA (full circles) and CT-DNA (empty diamonds). Measurements were performed by using 10 μM of complex in 50 mM Tris•HCl buffer, with 50 mM NaCl at pH 7.4 under ambient air conditions. The fitted curved were obtained by using a modified McGhee–von Hippel equation and drawn as solid and dashed curves for SS- and CT-DNA, respectively.

Table 4. Binding affinity constants calculated for complexes **1**–**3** with SS-DNA and CT-DNA.

	SS-DNA		CT-DNA	
	K_{aff} [L mol^{-1}][a]	I/I_0 max	K_{aff} [L mol^{-1}][a]	I/I_0 max
Ru-DPAC	1.8×10^6	2.6	4.2×10^5	2.8
Ru-DPACF_2	4.8×10^5	3.0	3.7×10^5	3.2
Ru-DPACF_4	3.5×10^5	2.9	1.5×10^5	3.1

[a] Binding constant were obtained by using a McGhee–von Hippel-type equation; the binding site was fixed to two base pairs per complex (best fit). Errors estimated to 5 %.

Even if these two natural DNAs contain nearly the same content of G–C base pairs (43 % for SS-DNA vs. 42 % for CT-DNA),[44] the luminescence behavior is slightly different for the complexes **1**–**3** in the presence of each DNA. Such an observation could arise from the different topologies of these two DNAs: CT-DNA features a long and well-defined scaffold (> 10 000 base pairs),[45] whereas SS-DNA is made of shorter (ca. 2000 base pairs)[46] and poorly defined sequences. The interaction between the complexes and the DNA sequences depends on the local environment encountered by the intercalated complex;[47] the heterogeneity of these environments results in small but noticeable differences in the optical properties of the complexes. The binding curves obtained are thus affected by this heterogeneity, but overall the binding constants calculated are in good agreement with an intercalation mode of interaction between each of our complexes and DNA.

In the case of SS-DNA, the emission intensity increases quickly to reach a plateau value, between 2.6 and 2.9 for the three complexes, the fluorinated analogs **2** and **3** display slightly higher I/I_0 values than the non-fluorinated complex **1**.

We also investigated the ability of Ru-DPAC to detect base mismatches in short oligonucleotides by using a series of hairpins oligonucleotide containing a mismatch near the center of the duplex (see sequences in Figure 6). As shown in Figure 7, an attenuation of the luminescence is observed for the mismatched hairpins with respect to the complementary one. No

differential luminescence intensity occurs related to the nature of the mismatch. The absence of specificity for the nature of the mismatch sites, and, more surprisingly, the lower luminescence enhancement of the complex in the presence of mismatched hairpins compared with the complementary one led us to the conclusion that Ru-DPAC is less effectively intercalated between the mismatched base pair stack. This less effective intercalation results in increased exposure to oxygen with respect to the complementary sites; a looser fit of the complex within the mismatch site favors non-radiative relaxation pathways of the excited state, leading to a decreased luminescence and/or a lower binding affinity for these sites compared with complementary sites. As saturation of the interaction between the complex and the hairpins cannot be obtained, it is difficult to differentiate the processes at stake in this case. The behavior observed for Ru-DPAC differs from the one reported for Ru-DPPZ[9] under the same conditions. This fundamental difference underlines the complexity of designing complexes able to probe mismatched sites in DNA.

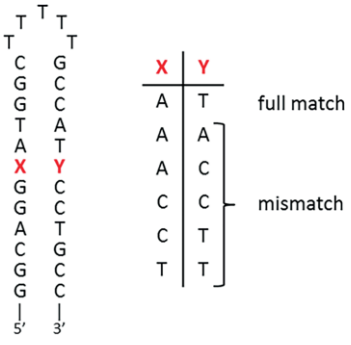

Figure 6. Hairpin oligonucleotide sequences used for titrations.

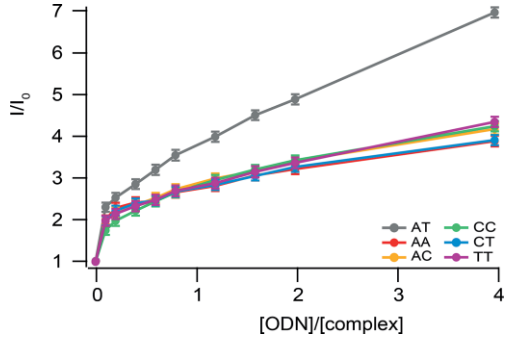

Figure 7. Oligonucleotides possessing (or not) a mismatched base pair. Measurements were performed by using 1 μM of complex in 5 mM Tris·HCl buffer, with 1 mM NaCl, at pH 7.5 under ambient air conditions.

Conclusions

We successfully synthesized and characterized new Ru^{II} complexes with extended planar ligands based on an acridine core. Their spectroscopic and electrochemical data revealed that **1**–**2** allow emission from an $^3MLCT_{phen/dpac}$ excited state, which explain the similarity of the luminescence maxima. As only minor reorganizations of the different triplet excited states of **1**–**2** occur in water, these compounds behave like $[Ru(phen)_3]^{2+}$ and exhibit increased luminescence in this solvent. However, the lowest ^3MLCT state for Ru-DPACF$_4$ changes from a bright $^3MLCT_{phen/dpac}$ state to a poorly luminescent $^3MLCT_{dpac}$ state. The stabilization of this state compared with the other ^3MLCT states occurs in water through the establishment of a hydrogen bond; the relative population of the excited state is then shifted to this state and the emissive $^3MLCT_{phen/dpac}$ states are less populated, yielding a reduction of the luminescence of Ru-DPACF$_4$ in water compared with organic solvents.

Studies of these acridine-based complexes in the presence of DNA demonstrate that they strongly bind to polynucleotides and that this association, attributed to an intercalation within the base pair stacking, is accompanied by an enhancement in their luminescence. This enhancement is presumably due to a decrease in the non-radiative deactivation processes of the ^3MLCT excited state of complexes intercalated in the double helix, where the microenvironment protects them from quenching by oxygen. In the case of Ru-DPACF$_4$, an inhibition of hydrogen bonds between the tetrafluoroacridine and water is likely to be responsible for the luminescence enhancement upon intercalation through DNA; this process is the same as the one responsible for the light-switching behavior of the well-known Ru-DPPZ complex. Ru-DPAC shows differential luminescence intensity for matched and mismatched hairpins, but no discrimination for the nature of the mismatch site. We suggest that a looser fit to the mismatched containing hairpins lies at the basis of the observed luminescence behavior of this complex, resulting in an increased exposure to oxygen with respect to the complementary sites. The design of extended planar ligands allowing better differential interactions between their corresponding Ru^{II} complexes and polynucleotides is currently under investigation in our group.

Experimental Section

Materials and Instrumentation: $[Ru(phen)_2Cl_2]$[13] was synthesized according to a previously described literature protocol. All solvents and reagents for the synthesis were of reagent grade and were used without any further purification. All solvents for the spectroscopic and electrochemical measurements were of spectroscopic grade. Water was purified with a Millipore Milli-Q system. Calf thymus DNA type I (CT-DNA) and salmon sperm DNA (SS-DNA) were purchased from Sigma–Aldrich. Hairpin oligonucleotides (ODNs) were purchased from Eurogentec. DNA and ODN concentrations were determined spectroscopically ($\lambda_{260\ nm}$ = 6600 $M^{-1}\ cm^{-1}$/bp for CT-DNA and SS-DNA;[14] $\lambda_{260\ nm}$ = 260 000 $M^{-1}\ cm^{-1}$ for ODN-AT, 264 900 $M^{-1}\ cm^{-1}$ for ODN-AA, 253 300 $M^{-1}\ cm^{-1}$ for ODN-CC, 259 100 $M^{-1}\ cm^{-1}$ for ODN-AC, 254 200 $M^{-1}\ cm^{-1}$ for ODN-CT, and 257 500 $M^{-1}\ cm^{-1}$ for ODN-TT). The molar extinction coefficients of the hairpin oligonucleotides were calculated based on the base content of each sequence. ^1H NMR experiments were performed in $CDCl_3$, CD_3OD, or CD_3CN with a Bruker AC-300 Avance II (300 MHz) or a Bruker AM-500 (500 MHz) at 20 °C. The chemical shifts (given in ppm) are measured versus the residual peak of the solvent as the internal standard. High-resolution mass spectrometry (HRMS) spectra were recorded with a Q-Extractive orbitrap from Thermo-Fisher by using reserpine as the internal standard. Samples were ionized by electrospray ionization (ESI; capillary temperature = 320 °C, vaporizer temperature = 320 °C, sheath gas flow rate = 5 mL

min^{-1}). UV/Vis absorption spectra were recorded with a Shimadzu UV-1700. Room temperature fluorescence spectra were recorded with a Varian Cary Eclipse instrument. Luminescence intensity at 77 K was recorded with a FluoroLog3 FL3–22 from Jobin Yvon equipped with an 18 V 450 W Xenon Short Arc lamp and an R928P photomultiplier, using an Oxford Instrument Optistat DN nitrogen cryostat controlled by an Oxford Intelligent Temperature Controller (ITC503S) instrument. For the luminescence lifetime measurements as a function of temperature, the pulsed excitation source was a pulsed laser Nd:YAG Q-switched laser (Continuum Inc.) frequency-tripled (355 nm) coupled with an optical parametric oscillator (Continuum Inc.) covering the wavelength region 410–2300 nm with a maximum pulse energy from 10 to 120 mJ depending on the wavelength. The emission was detected perpendicularly by a photomultiplier (R928, Hamamatsu). The signal was recorded with a digital oscilloscope (HP 54200A), connected through the IEEE488 interface to a personal computer, and was averaged over at least 16 shots. The emission wavelength was selected by a grating Czerny–Turner monochromator (Spectra Pro 2300i, Acton Research Corp.). Cyclic voltammetry was carried out in a one-compartment cell, using a glassy carbon disk working electrode (approximate area = 0.03 cm^2), a platinum wire counter electrode, and an Ag/AgCl reference electrode (salt bridge: 3 mol L^{-1} NaCl/saturated AgCl). The potential of the working electrode was controlled by an Autolab PGSTAT 100 potentiostat through a PC interface. The cyclic voltammograms were recorded with a sweep rate of 300 mV s^{-1}, in dried acetonitrile or *N*,*N*-dimethylformamide (Sigma–Aldrich, HPLC grade). The concentration of the complexes was 8×10^{-4} mol L^{-1}, with 0.1 mol L^{-1} tetrabutylammonium perchlorate as supporting electrolyte. Before each measurement, the samples were purged with nitrogen. The molar absorption coefficients were determined by ^{1}H NMR spectroscopy by using 2,2′-[(perfluoroethane-1,2-diyl)bis(oxy)]bis(2,2-difluoroethan-1-ol) as a reference. DFT calculations were performed by using Gaussian 09.[15] The hybrid functional PBE0 was used to carry out the DFT[16] and TD-DFT[17] calculations in combination with the LanL2DZ[18] basis set for all atoms. Geometry optimizations were conducted without symmetry constraints. Frequency calculations on each optimized structure confirmed that the energy minima was reached. The energy, oscillator strength, and related MO contributions for the 100 lowest singlet–singlet and ten lowest singlet–triplet excitations for the S_0-optimized geometry were obtained, respectively, from the TD-DFT/singlets and the TD-DFT/triplets output files. One should note that the PBE0 functional, although providing the correct excitation energies, is not able to fully reproduce their relative intensities. This behavior has already been noticed in the literature in the case of even simpler compounds and different functionals and more elaborated approaches have been used in cases where the band shape is of interest, which was actually not the case in the present study.[19] GaussView 3.0.9,[20] GaussSum 3.0,[21] and Chemissian 4.38[22] software were used for data analysis, visualization, and surface plots. Calculations were performed in MeCN or H_2O solution by use of the conductor-like polarized continuum (CPCM) solvation model as implemented in Gaussian 09.[15] Because the continuum model could not describe specific interactions such as nitrogen–hydrogen-bond interactions, a discrete model is also used in an approach similar to that reported by Daniel et al. recently.[23]

Synthetic Procedures and Characterization of dpac Ligands and Respective Ru^{II} Complexes

2-Aminobenzyl Alcohol: A solution of $LiAlH_4$ in dry Et_2O (300.0 mg in 7.5 mL) was added dropwise to a solution of anthranilic acid (617.3 mg, 4.50 mmol) in dry Et_2O (30 mL). The mixture was then stirred at reflux (35 °C) for 1 h. After cooling to room temperature, EtOAc (25 mL) was added, followed by a solution of NaOH 2 M until effervescence stops, and MilliQ water (40 mL). The organic phase was separated and the aqueous phase was extracted with Et_2O (3 × 30 mL). The combined organic phases were dried with $MgSO_4$, evaporated, and dried under vacuum. The desired compound was obtained as a beige solid, yield 93 %. ^{1}H NMR (300 MHz, $CDCl_3$): δ = 7.15 (ddd, $J_{c\text{-}d}$ = 8.0, $J_{c\text{-}b}$ = 8.0, $J_{c\text{-}a}$ = 1.6 Hz, 1 H, H_c), 7.07 (dd, $J_{a\text{-}b}$ = 7.6, $J_{a\text{-}c}$ = 1.6 Hz, 1 H, H_a), 6.70–6.75 (m, 2 H, H_b and H_d), 4.70 (s, 2 H, CH_2), 3.19 (br., 2 H, NH_2) ppm.

dpac (4): 5-Amino-1,10-phenanthroline (183.0 mg, 0.938 mmol) and 2-aminobenzyl alcohol (115.6 mg, 0.938 mmol) were suspended in 6 N HCl (3.0 mL). The reaction mixture was stirred at reflux (65 °C) for 20 h and, after cooling to room temperature, the reaction was quenched by addition of NH_3•H_2O until reaching pH 9. The orange precipitate was filtered and purified by using a neutral alumina column for chromatography (eluent: acetone/methanol gradient, from 100:0 to 90:10), yielding the targeted compound as a dark-orange solid, yield 93 %. ^{1}H NMR (500 MHz, CD_3OD): δ = 9.77 (dd, $J_{c\text{-}b}$ = 8.3, $J_{c\text{-}a}$ = 1.8 Hz, 1 H, H_c), 9.68 (s, 1 H, H_d), 9.30 (dd, $J_{i\text{-}j}$ = 8.3, $J_{i\text{-}k}$ = 1.5 Hz, 1 H, H_i), 9.14 (dd, $J_{a\text{-}b}$ = 4.5, $J_{a\text{-}c}$ = 1.8 Hz, 1 H, H_a), 9.08 (dd, $J_{k\text{-}j}$ = 4.5, $J_{k\text{-}i}$ = 1.6 Hz, 1 H, H_k), 8.34 (d, $J_{e\text{-}f}$ = 8.7 Hz, 1 H, H_e), 8.26 (d, $J_{h\text{-}g}$ = 7.6 Hz, 1 H, H_h), 7.95 (dd, $J_{f\text{-}e}$ = 8.5, $J_{f\text{-}g}$ = 6.9 Hz, 1 H, H_f), 7.89 (2dd, $J_{b\text{-}c}$ = $J_{j\text{-}l}$ = 8.0, $J_{b\text{-}a}$ = $J_{j\text{-}k}$ = 4.5 Hz, 2 H, H_b and H_j), 7.76 (t, $J_{g\text{-}h}$ = 7.2 Hz, 1 H, H_g) ppm. MS (APCI, +c): calcd. 282.10 for $C_{19}H_{12}N_3$, found 282.27 [M + H$^+$].

(2-Amino-4,5-difluorophenyl)methanol: A solution of $LiAlH_4$ in dry Et_2O (78.5 mg in 2.0 mL) was added dropwise to a solution of 4,5-difluoroanthranilic acid (200.0 mg, 1.155 mmol) in dry Et_2O (8.0 mL). The mixture was then stirred at reflux (35 °C) for 1 h 15 min. After cooling to room temperature, EtOAc (10 mL) was added, followed by a solution of NaOH (2 M) until effervescence stopped, and MilliQ water (15 mL). The organic phase was separated and the aqueous phase was extracted with Et_2O (3 × 10 mL). The combined organic phases were dried with $MgSO_4$, evaporated, and dried under vacuum. The desired compound was obtained as a flaky yellowish-brownish solid, yield 91 %. ^{1}H NMR (300 MHz, $CDCl_3$): δ = 6.92 (dd, $J_{a\text{-}b}$ = 10.5, $J_{a\text{-}c}$ = 8.6 Hz, 1 H, H_a), 6.50 (dd, $J_{d\text{-}c}$ = 11.8, $J_{d\text{-}b}$ = 6.8 Hz, 1 H, H_d), 4.61 (s, 2 H, CH_2), 4.12 (br., 2 H, NH_2) ppm.

dpacF_2 (5): 5-Amino-1,10-phenanthroline (50.0 mg, 0.256 mmol) and (2-amino-4,5-difluorophenyl)methanol (40.8 mg, 0.256 mmol) were suspended in 6 N HCl (1.0 mL). The reaction mixture was stirred at reflux (65 °C) for 20 h and, after cooling to room temperature, the reaction was quenched by addition of NH_3•H_2O until reaching pH 9. The orange-red precipitate was filtered and purified by using a neutral alumina column for chromatography (eluent: acetone/methanol gradient, from 100:0 to 90:10), yielding the targeted compound as an orange solid, yield 98 %. ^{1}H NMR (300 MHz, $CDCl_3$): δ = 9.70 (dd, $J_{c\text{-}b}$ = 8.2, $J_{c\text{-}a}$ = 1.9 Hz, 1 H, H_c), 9.27 (dd, $J_{a\text{-}b}$ = 4.5, $J_{a\text{-}c}$ = 1.8 Hz, 1 H, H_a), 9.25 (s, 1 H, H_d), 9.23 (dd, $J_{k\text{-}j}$ = 4.4, $J_{k\text{-}i}$ = 1.5 Hz, 1 H, H_k), 8.96 (dd, $J_{i\text{-}j}$ = 8.3, $J_{i\text{-}k}$ = 1.6 Hz, 1 H, H_i), 8.10 (dd, $J_{e\text{-}f}$ = 10.9, $J_{e\text{-}g}$ = 7.6 Hz, 1 H, H_e), 7.78 (m, 3 H, H_b, H_j, and H_h) ppm. MS (APCI, +c): calcd. 318.08 for $C_{19}H_{10}F_2N_3$, found 318.55 [M + H$^+$].

(2-Amino-3,4,5,6-tetrafluorophenyl)methanol: A solution of $LiAlH_4$ in dry Et_2O (76.5 mg in 2.0 mL) was added dropwise to a solution of 2-amino-3,4,5,6-tetrafluorobenzoic acid (200.0 mg, 0.9565 mmol) in dry Et_2O (8.0 mL). The mixture was then stirred at reflux (35 °C) for 2 h 10 min. After cooling to room temperature, EtOAc (10 mL) was added, followed by a solution of NaOH (2 M) until effervescence stopped, and MilliQ water (15 mL). The organic phase was separated and the aqueous phase was extracted with Et_2O (3 × 10 mL). The combined organic phases were dried with $MgSO_4$, evaporated, and dried under vacuum. The desired com-

pound was obtained as a beige solid, yield 93 %. ^{1}H NMR (300 MHz, $CDCl_3$): δ = 4.78 (d, $J_{CH2\text{-}F}$ = 1.95 Hz, 2 H, CH_2), 3.63 (br., 2 H, NH_2) ppm.

dpacF$_4$ (6): 5-Amino-1,10-phenanthroline (167.1 mg, 0.8568 mmol) and (2-amino-3,4,5,6-tetrafluorophenyl)methanol (167.1 mg, 0.8568 mmol) were suspended in 6 N HCl (2.0 mL). The reaction mixture was stirred at reflux (65 °C) for 20 h and, after cooling to room temperature, the reaction was quenched by addition of NH_3•H_2O until reaching pH 9. The orange-red precipitate was filtered and purified by using a neutral alumina column for chromatography (eluent: acetone/methanol gradient, from 100:0 to 90:10). After evaporation of the solvents, the residue was washed with chloroform. The precipitate was filtered and the filtrate was evaporated, yielding the targeted compound as an orange-yellow solid, yield 94 %. ^{1}H NMR (300 MHz, $CDCl_3$): δ = 9.77 (dd, $J_{c\text{-}b}$ = 8.1, $J_{c\text{-}a}$ = 1.7 Hz, 1 H, H_c), 9.55 (s, 1 H, H_d), 9.31 (dd, $J_{a\text{-}b}$ = 4.5, $J_{a\text{-}c}$ = 1.7 Hz, 1 H, H_a), 9.27 (dd, $J_{k\text{-}j}$ = 4.4, $J_{k\text{-}i}$ = 1.5 Hz, 1 H, H_k), 9.05 (dd, $J_{i\text{-}j}$ = 8.2, $J_{i\text{-}k}$ = 1.5 Hz, 1 H, H_i), 7.83 (m, 2 H, H_b and H_j) ppm. MS (APCI, +c): calcd. 354.07 for $C_{19}H_8F_4N_3$, found 354.31 [M + H^+].

Ru-DPAC (1): One equivalent of dichloro precursor Ru(phen)$_2$Cl$_2$ (10.0 mg, 0.0188 mmol) was mixed with 1.2 equiv. of dpac (**4**) (6.9 mg, 0.024 mmol) in a mixture of absolute ethanol/water (50:50, 2.0 mL). The reaction mixture was stirred under an argon atmosphere at reflux (80 °C) and the reaction was followed by absorption spectroscopy. After 3 h, the medium was concentrated and addition of small portions of NH_4PF_6 and drops of water yielded a red precipitate. After centrifugation, the solid was washed with excess water. After drying under vacuum, the orange-red residue was purified by preparative plate chromatography (silica, eluent: CH_3CN/H_2O/saturated aqueous NH_4Cl 4:3:1, R_f = 0.30). The counter-anion exchange from PF_6 to Cl was performed by eluting a solution of the complex in a mixture of CH_3CN/H_2O on Sephadex DEAE A25. ^{1}H NMR (PF_6 salt, 500 MHz, CD_3CN): δ = 9.80 (s, 1 H, H_d), 9.73 (dd, $J_{i\text{-}j}$ = 8.2, $J_{i\text{-}k}$ = 1.3 Hz, 1 H, H_i), 9.25 (dd, $J_{c\text{-}b}$ = 8.4, $J_{c\text{-}a}$ = 1.2 Hz, 1 H, H_c), 8.61 (2dd, $J_{4\text{-}3}$ = $J_{7\text{-}8}$ = 8.7, $J_{4\text{-}2}$ = $J_{7\text{-}9}$ = 1.2 Hz, 4 H, H^4, $H^{4'}$, H^7, $H^{7'}$), 8.41 (d, $J_{f\text{-}e}$ = 8.6 Hz, 1 H, H_f), 8.35 (d, $J_{g\text{-}h}$ = 8.2 Hz, 1 H, H_g), 8.25 (AB system, 4 H, H^5, $H^{5'}$, H^6, $H^{6'}$), 8.20 (dd, $J_{a\text{-}b}$ = 5.3, $J_{a\text{-}c}$ = 1.2 Hz, 1 H, H_a), 8.19 (dd, $J_{k\text{-}j}$ = 5.3, $J_{k\text{-}i}$ = 1.3 Hz, 1 H, H_k), 8.03 (m, 5 H, H^2, $H^{2'}$, H^9, $H^{9'}$, H_h), 7.87 (d, $J_{e\text{-}f}$ = 8.6 Hz, 1 H, H_e), 7.64 (m, 6 H, H^3, $H^{3'}$, H^8, $H^{8'}$, H_b, H_j) ppm. HRMS (ESI, +p): calcd. 888.10078 for $[C_{43}H_{27}N_7F_6PRu]^+$, found 888.10167 ([$M$ – PF_6^-]$^+$) and calcd. 371.56802 for $[C_{43}H_{27}N_7Ru]^{2+}$, found 371.56835 ([M – 2 PF_6^-]$^{2+}$).

Ru-DPACF$_2$ (2): One equivalent of dichloro precursor Ru(phen)$_2$Cl$_2$ (10.0 mg, 0.0188 mmol) was mixed with 1.5 equiv. of dpacF$_2$ (**5**) (8.9 mg, 0.028 mmol) in a mixture of absolute ethanol/water (50:50, 2.0 mL). The reaction mixture was stirred under an argon atmosphere at reflux (80 °C) and the reaction was followed by absorption spectroscopy. After 3 h, the medium was concentrated and addition of small portions of NH_4PF_6 and drops of water yielded a red precipitate. After centrifugation, the solid was washed with excess water. After drying under vacuum, the orange-red residue was purified by preparative plate chromatography (silica, eluent: CH_3CN/H_2O/saturated aqueous NH_4Cl 4:3:1, R_f = 0.28). The counter-anion exchange from PF_6 to Cl was performed by eluting a solution of the complex in a mixture of CH_3CN/H_2O on Sephadex DEAE A25. ^{1}H NMR (PF_6 salt, 500 MHz, CD_3CN): δ = 9.77 (s, 1 H, H_d), 9.67 (dd, $J_{i\text{-}j}$ = 8.2, $J_{i\text{-}k}$ = 1.3 Hz, 1 H, H_i), 9.22 (dd, $J_{c\text{-}b}$ = 8.5, $J_{c\text{-}a}$ = 1.1 Hz, 1 H, H_c), 8.61 (2dd, $J_{4\text{-}3}$ = $J_{7\text{-}8}$ = 8.5, $J_{4\text{-}2}$ = $J_{7\text{-}9}$ = 1.3 Hz, 4 H, H^4, $H^{4'}$, H^7, $H^{7'}$), 8.26 (AB system, 4 H, H^5, $H^{5'}$, H^6, $H^{6'}$), 8.17 (m, 4 H, H_e, H_h, H^2, $H^{2'}$), 8.06 (dd, $J_{k\text{-}j}$ = 5.3, $J_{k\text{-}i}$ = 1.3 Hz, 1 H, H_k), 8.01 (m, 3 H, H_a, H^9, $H^{9'}$), 7.72 (2 dd, $J_{3\text{-}4/3'\text{-}4'}$ = $J_{8\text{-}7/8'\text{-}7'}$ = 8.3, $J_{3\text{-}2/3'\text{-}2'}$ = $J_{8\text{-}9/8'\text{-}9'}$ = 5.4 Hz, 2 H, $H^{3/3'}$, $H^{8/8'}$), 7.63 (m, 4 H, $H^{3/3'}$, $H^{8/8'}$, H_b, H_j) ppm. HRMS (ESI, +p): calcd. 924.08193 for $[C_{43}H_{25}N_7F_8PRu]^+$, found 924.08240 ([$M$ – PF_6^-]$^+$) and calcd. 389.55860 for $[C_{43}H_{25}N_7F_2Ru]^{2+}$, found 389.55897 ([$M$ – 2 PF_6^-]$^{2+}$).

Ru-DPACF$_4$ (3): One equivalent of dichloro precursor Ru(phen)$_2$Cl$_2$ (11.6 mg, 0.0218 mmol) was mixed with 1.3 equiv. of dpacF$_4$ (**6**) (10.0 mg, 0.0283 mmol) in a mixture of absolute ethanol/water (50:50, 2.0 mL). The reaction mixture was stirred under an argon atmosphere at reflux (80 °C) and the reaction was followed by absorption spectroscopy. After 2 h 30 min, the medium was concentrated and addition of small portions of NH_4PF_6 and drops of water yielded a red precipitate. After centrifugation, the solid was washed with excess water. After drying under vacuum, the orange-red residue was purified by HPLC (XBridge C18 10 × 100 mm, 5 µM, gradient from H_2O/CH_3CN, 90:10 + 0.1 % TFA to CH_3CN + 0.1 % TFA, elution time: 3.07 min). The counter-anion exchange from PF_6 to Cl was performed by eluting a solution of the complex in a mixture of CH_3CN/H_2O on Sephadex DEAE A25. ^{1}H NMR (PF_6 salt, 500 MHz, CD_3CN): δ = 9.97 (s, 1 H, H_d), 9.68 (dd, $J_{i\text{-}j}$ = 8.3, $J_{i\text{-}k}$ = 1.3 Hz, 1 H, H_i), 9.33 (dd, $J_{c\text{-}b}$ = 7.5, $J_{c\text{-}a}$ = 1.0 Hz, 1 H, H_c), 8.61 (2dd, $J_{4\text{-}3}$ = $J_{7\text{-}8}$ = 8.6, $J_{4\text{-}2}$ = $J_{7\text{-}9}$ = 1.2 Hz, 4 H, H^4, $H^{4'}$, H^7, $H^{7'}$), 8.26 (AB system, 4 H, H^5, $H^{5'}$, H^6, $H^{6'}$), 8.19 (dd, $J_{2\text{-}3}$ = 5.2, $J_{2\text{-}4}$ = 1.2 Hz, 1 H, $H^{2/2'}$), 8.16 (dd, $J_{9\text{-}8}$ = 5.3, $J_{9\text{-}7}$ = 1.2 Hz, 1 H, $H^{9/9'}$), 8.10 (dd, $J_{k\text{-}j}$ = 5.3, $J_{k\text{-}i}$ = 1.3 Hz, 1 H, H_k), 8.04 (dd, $J_{a\text{-}b}$ = 5.4, $J_{a\text{-}c}$ = 1.0 Hz, 1 H, H_a), 8.00 (m, 2 H, $H^{2/2'}$, $H^{9/9'}$), 7.73 (2dd, $J_{b\text{-}a}$ = $J_{j\text{-}k}$ = 5.4, $J_{b\text{-}c}$ = $J_{j\text{-}i}$ = 8.3 Hz, 2 H, H_b, H_j), 7.65 (m, 4 H, H^3, $H^{3'}$, H^8, $H^{8'}$) ppm. HRMS (ESI, +p): calcd. 960.06309 for $[C_{43}H_{23}N_7F_{10}PRu]^+$, found 960.06347 ([$M$ – PF_6^-]$^+$) and calcd. 407.54918 for $[C_{43}H_{23}N_7F_4Ru]^{2+}$, found 407.54953 ([$M$ – 2 PF_6^-]$^{2+}$).

Acknowledgments

Q. D. and B. E. gratefully acknowledge the Université Catholique de Louvain, the Fonds National pour la Recherche Scientifique (FRS-FNRS), the Région Wallonne, and the Fondation Louvain (Prix Pierre et Colette Bauchau) for financial support. This research was enabled in part by support provided by WestGrid (www.westgrid.ca) and Compute Canada Calcul Canada (www.computecanada.ca). L. M. thanks the Belgian American Educational Foundation (BAEF) for the Cabeaux–Jacobs Fellowship. F. L. thanks the Labex Arcane, France (ANR-11-LABX-0003-01) and the chemistry platform NanoBio campus in Grenoble for luminescence lifetime measurement facilities. Q. D. also warmly thanks Laurent Collard, Cédric Lentz, Christophe Rubay, and Stéphanie Wautier for their scientific help.

Keywords: Photophysics · DNA · DNA recognition · Ruthenium · Acridine

[1] a) Z. Guo, P. J. Sadler, *Angew. Chem. Int. Ed.* **1999**, *38*, 1512–1531; *Angew. Chem.* **1999**, *111*, 1610–1630; b) C. Orvig, M. J. Abrams, *Chem. Rev.* **1999**, *99*, 2201–2204; c) K. K.-W. Lo, *Photofunctional Transition Metal Complexes*, vol. 123, Springer, Berlin/Heidelberg, Germany, **2007**, p. 205–245.

[2] a) F. Puntoriero, A. Sartorel, M. Orlandi, G. La Ganga, S. Serroni, M. Bonchio, F. Scandola, S. Campagna, *Coord. Chem. Rev.* **2011**, *255*, 2594–2601; b) H. Ozawa, K. Sakai, *Chem. Commun.* **2011**, *47*, 2227–2242.

[3] a) J. J. Concepcion, J. W. Jurss, M. K. Brennaman, P. G. Hoertz, A. O. Patrocinio, N. Y. Murakami Iha, J. L. Templeton, T. J. Meyer, *Acc. Chem. Res.* **2009**, *42*, 1954–1965; b) M. K. Nazeeruddin, S. M. Zakeeruddin, J. J. Lagref, P. Liska, P. Comte, C. Barolo, G. Viscardi, K. Schenk, M. Graetzel, *Coord. Chem. Rev.* **2004**, *248*, 1317–1328; c) L. Troian-Gautier, C. Moucheron, *Molecules* **2014**, *19*, 5028–5087.

[4] a) M. R. Gill, J. A. Thomas, *Chem. Soc. Rev.* **2012**, *41*, 3179–3192; b) A. W. McKinley, P. Lincoln, E. M. Tuite, *Coord. Chem. Rev.* **2011**, *255*, 2676–2692; c) A. C. Komor, J. K. Barton, *Chem. Commun.* **2013**, *49*, 3617–3630.
[5] a) L. Marcélis, J. Ghesquière, K. Garnir, A. Kirsch-De Mesmaeker, C. Moucheron, *Coord. Chem. Rev.* **2012**, *256*, 1569–1582; b) L. Marcelis, C. Moucheron, A. Kirsch-De Mesmaeker, *Philos. Trans. R. Soc. London, Ser. A* **2013**, *371*, 20120131.
[6] A. E. Friedman, J. C. Chambron, J. P. Sauvage, N. J. Turro, J. K. Barton, *J. Am. Chem. Soc.* **1990**, *112*, 4960–4962.
[7] a) J. Olofsson, L. M. Wilhelmsson, P. Lincoln, *J. Am. Chem. Soc.* **2004**, *126*, 15458–15465; b) E. J. C. Olson, D. Hu, A. Hörmann, A. M. Jonkman, M. R. Arkin, E. D. A. Stemp, J. K. Barton, P. F. Barbara, *J. Am. Chem. Soc.* **1997**, *119*, 11458–11467; c) B. Onfelt, P. Lincoln, B. Norden, J. S. Baskin, A. H. Zewail, *Proc. Natl. Acad. Sci. USA* **2000**, *97*, 5708–5713; d) M. K. Brennaman, T. J. Meyer, J. M. Papanikolas, *J. Phys. Chem. A* **2004**, *108*, 9938–9944.
[8] C. Turro, S. H. Bossmann, Y. Jenkins, J. K. Barton, N. J. Turro, *J. Am. Chem. Soc.* **1995**, *117*, 9026–9032.
[9] M. H. Lim, H. Song, E. D. Olmon, E. E. Dervan, J. K. Barton, *Inorg. Chem.* **2009**, *48*, 5392–5397.
[10] M. Demeunynck, C. Moucheron, A. Kirsch-De Mesmaeker, *Tetrahedron Lett.* **2002**, *43*, 261–264.
[11] a) B. Elias, L. Herman, C. Moucheron, A. Kirsch-De Mesmaeker, *Inorg. Chem.* **2007**, *46*, 4979–4988; b) L. Herman, B. Elias, F. Pierard, C. Moucheron, A. Kirsch-De Mesmaeker, *J. Phys. Chem. A* **2007**, *111*, 9756–9763.
[12] K. Kobayashi, H. Ohtsu, K. Nozaki, S. Kitagawa, K. Tanaka, *Inorg. Chem.* **2016**, *55*, 2076–2084.
[13] L. Jacquet, A. Kirsch-De Mesmaeker, *Faraday Trans.* **1992**, *88*, 2471–2480.
[14] a) E. M. Castanheira, M. S. Carvalho, A. R. Rodrigues, R. C. Calhelha, M. J. Queiroz, *Nanoscale Res. Lett.* **2011**, *6*, 379–387; b) R. B. Dixit, T. S. Patel, S. F. Vanparia, A. P. Kunjadiya, H. R. Keharia, B. C. Dixit, *Sci. Pharm.* **2011**, *79*, 293–308.
[15] M. J. Frisch, G. W. Trucks, H. B. Schlegel, G. E. Scuseria, M. A. Robb, J. R. Cheeseman, G. Scalmani, V. Barone, B. Mennucci, G. A. Petersson, H. Nakatsuji, M. Caricato, X. Li, H. P. Hratchian, A. F. Izmaylov, J. Bloino, G. Zheng, J. L. Sonnenberg, M. Hada, M. Ehara, K. Toyota, R. Fukuda, J. Hasegawa, M. Ishida, T. Nakajima, Y. Honda, O. Kitao, H. Nakai, T. Vreven, J. A. Montgomery Jr., J. E. Peralta, F. Ogliaro, M. Bearpark, J. J. Heyd, E. Brothers, K. N. Kudin, V. N. Staroverov, R. Kobayashi, J. Normand, K. Raghavachari, A. Rendell, J. C. Burant, S. S. Iyengar, J. Tomasi, M. Cossi, N. Rega, J. M. Millam, M. Klene, J. E. Knox, J. B. Cross, V. Bakken, C. Adamo, J. Jaramillo, R. Gomperts, R. E. Stratmann, O. Yazyev, A. J. Austin, R. Cammi, C. Pomelli, J. W. Ochterski, R. L. Martin, K. Morokuma, V. G. Zakrzewski, G. A. Voth, P. Salvador, J. J. Dannenberg, S. Dapprich, A. D. Daniels, Ö. Farkas, J. B. Foresman, J. V. Ortiz, J. Cioslowski, D. J. Fox, *Gaussian 09*, revision D.01, Gaussian, Inc., Wallingford, CT, **2009**.
[16] a) P. Hohenberg, W. Kohn, *Phys. Rev.* **1964**, *136*, 864–871; b) W. Kohn, L. J. Sham, *Phys. Rev.* **1965**, *140*, 1133–1138; c) J. Reinhold, *Cryst. Res. Technol.* **1990**, *25*, 624; d) R. G. Parr, W. Yang, *Density Functional Theory of Atoms and Molecules*, vol. 16, Oxford University Press, Oxford, UK, **1989**.
[17] a) R. E. Stratmann, G. E. Scuseria, M. J. Frisch, *J. Chem. Phys.* **1998**, *109*, 8218–8224; b) R. Bauernschmitt, R. Ahlrichs, *Chem. Phys. Lett.* **1996**, *256*, 454–464; c) M. E. Casida, C. Jamorski, K. C. Casida, D. R. Salahub, *J. Chem. Phys.* **1998**, *108*, 4439–4449.
[18] a) T. H. Dunning Jr., P. J. Hay, *Modern Theoretical Chemistry*, 3rd edition, Plenum, New York, **1977**; b) P. J. Hay, W. R. Wadt, *J. Chem. Phys.* **1985**, *82*, 270–283; c) W. R. Wadt, P. J. Hay, *J. Chem. Phys.* **1985**, *82*, 284–298; d) P. J. Hay, W. R. Wadt, *J. Chem. Phys.* **1985**, *82*, 299–310.
[19] A. Charaf-Eddin, A. Planchat, B. Mennucci, C. Adamo, D. Jacquemin, *J. Chem. Theory Comput.* **2013**, *9*, 2749–2760.
[20] R. D. K. Dennington II, T. Keith, J. Millam, K. Eppinnett, W. L. Hovell, R. Gilliland, *GaussView* 3.09, Semichem, Inc., Shawnee Mission, KS, **2003**.
[21] N. M. O'Boyle, A. L. Tenderholt, K. M. Langner, *J. Comput. Chem.* **2008**, *29*, 839–845.
[22] L. Skripnikov, *Chemissian*, V4.38, **2005**–**2015**.
[23] T. Very, D. Ambrosek, M. Otsuka, C. Gourlaouen, X. Assfeld, A. Monari, C. Daniel, *Chem. Eur. J.* **2014**, *20*, 12901–12909.
[24] N. Busto, J. Valladolid, M. Martinez-Alonso, H. J. Lozano, F. A. Jalon, B. R. Manzano, A. M. Rodriguez, M. C. Carrion, T. Biver, J. M. Leal, G. Espino, B. Garcia, *Inorg. Chem.* **2013**, *52*, 9962–9974.
[25] a) S. V. Ley, A. W. Thomas, *Angew. Chem. Int. Ed.* **2003**, *42*, 5400–5449; *Angew. Chem.* **2003**, *115*, 5558–5607; b) J. Lindley, *Tetrahedron* **1984**, *40*, 1433–1456; c) A. Ehrentraut, A. Zapf, M. Beller, *J. Mol. Catal. A* **2002**, *182–183*, 515–523; d) J. P. Wolfe, S. Wagaw, S. L. Buchwald, *J. Am. Chem. Soc.* **1996**, *118*, 7215–7216.
[26] a) D. C. Rogness, R. C. Larock, *J. Org. Chem.* **2010**, *75*, 2289–2295; b) H. Yoshida, Y. Asatsu, Y. Mimura, Y. Ito, J. Ohshita, K. Takaki, *Angew. Chem. Int. Ed.* **2011**, *50*, 9676–9679; *Angew. Chem.* **2011**, *123*, 9850–9853.
[27] F. Charmantray, M. Demeunynck, J. Lhomme, A. Duflos, *J. Org. Chem.* **2001**, *66*, 8222–8226.
[28] A. Juris, V. Balzani, F. Barigelletti, S. Campagna, P. Belser, A. von Zelewsky, *Coord. Chem. Rev.* **1988**, *84*, 85–277.
[29] E. Amouyal, A. Homsi, J.-C. Chambron, J.-P. Sauvage, *J. Chem. Soc., Dalton Trans.* **1990**, 1841–1845.
[30] I. Ortmans, B. Elias, J. M. Kelly, C. Moucheron, A. Kirsch-De Mesmaeker, *Dalton Trans.* **2004**, 668–676.
[31] A. Vogler, *Ber. Bunsen-Ges. Phys. Chem.* **1991**, *95*, 1161.
[32] a) C. G. Coates, L. Jacquet, J. J. McGarvey, S. E. J. Bell, A. H. R. Al-Obaidi, J. M. Kelly, *J. Am. Chem. Soc.* **1997**, *119*, 7130–7136; b) R. M. Hartshorn, J. K. Barton, *J. Am. Chem. Soc.* **1992**, *114*, 5919–5925.
[33] M. Cossi, N. Rega, G. Scalmani, V. Barone, *J. Comput. Chem.* **2003**, *24*, 669–681.
[34] R. L. Martin, *J. Chem. Phys.* **2003**, *118*, 4775–4777.
[35] D. Garcia-Fresnadillo, Y. Georgiadou, G. Orellana, A. M. Braun, E. Oliveros, *Helv. Chim. Acta* **1996**, *79*, 1222–1238.
[36] a) G. Pourtois, D. Beljonne, C. Moucheron, S. Schumm, A. Kirsch-De Mesmaeker, R. Lazzaroni, J. L. Bredas, *J. Am. Chem. Soc.* **2004**, *126*, 683–692; b) J. Olofsson, B. Önfelt, P. Lincoln, *J. Phys. Chem. A* **2004**, *108*, 4391–4398.
[37] Y. Kawanishi, N. Kitamura, S. Tazuke, *Inorg. Chem.* **1989**, *28*, 2968–2975.
[38] a) C. Daniel, *Coord. Chem. Rev.* **2015**, *282–283*, 19–32; b) F. E. Poynton, J. P. Hall, P. M. Keane, C. Schwarz, I. V. Sazanovich, M. Towrie, T. Gunnlaugsson, C. J. Cardin, D. J. Cardin, S. J. Quinn, C. Long, J. M. Kelly, *Chem. Sci.* **2016**, *7*, 3075–3084; c) A. Chantzis, T. Very, C. Daniel, A. Monari, X. Assfeld, *Chem. Phys. Lett.* **2013**, *578*, 133–137; d) T. Very, S. Despax, P. Hebraud, A. Monari, X. Assfeld, *Phys. Chem. Chem. Phys.* **2012**, *14*, 12496–12504.
[39] M. Atsumi, L. González, C. Daniel, *J. Photochem. Photobiol. A* **2007**, *190*, 310–320.
[40] a) A. C. Bhasikuttan, M. Suzuki, S. Nakashima, T. Okada, *J. Am. Chem. Soc.* **2002**, *124*, 8398–8405; b) A. Cannizzo, F. van Mourik, W. Gawelda, G. Zgrablic, C. Bressler, M. Chergui, *Angew. Chem. Int. Ed.* **2006**, *45*, 3174–3176; *Angew. Chem.* **2006**, *118*, 3246–3248.
[41] S. Rickling, L. Ghisdavu, F. Pierard, P. Gerbaux, M. Surin, P. Murat, E. Defrancq, C. Moucheron, A. Kirsch-De Mesmaeker, *Chem. Eur. J.* **2010**, *16*, 3951–3961.
[42] C. Moucheron, A. Kirsch-De Mesmaeker, S. Choua, *Inorg. Chem.* **1997**, *36*, 584–592.
[43] J. D. McGhee, P. H. von Hippel, *J. Mol. Biol.* **1974**, *86*, 469–489.
[44] J. G. Stuart, J. J. Ferretti, *Can. J. Microbiol.* **1975**, *21*, 722–724.
[45] B. Porsch, R. Laga, J. Horsky, C. Konak, K. Ulbrich, *Biomacromolecules* **2009**, *10*, 3148–3150.
[46] K. Tanaka, Y. Okahata, *J. Am. Chem. Soc.* **1996**, *118*, 10679–10683.
[47] a) P. M. Keane, F. E. Poynton, J. P. Hall, I. V. Sazanovich, M. Towrie, T. Gunnlaugsson, S. J. Quinn, C. J. Cardin, J. M. Kelly, *Angew. Chem. Int. Ed.* **2015**, *54*, 8364–8368; *Angew. Chem.* **2015**, *127*, 8484–8488; b) J. A. Smith, M. W. George, J. M. Kelly, *Coord. Chem. Rev.* **2011**, *255*, 2666–2675.

Received: April 22, 2016
Published Online: July 14, 2016

